Effect of halloysite nanotubes filler on polydopamine properties

Marina Massaro,[a] Francesco Armetta,[a] Giuseppe Cavallaro,[b] Delia F. Chillura Martino,[b] Michelangelo Gruttadauria,[a] Giuseppe Lazzara,[b] Serena Riela[a,*] and Marco d'Ischia[c]

[a] Dipartimento STEBICEF, Sez. Chimica, Università degli Studi di Palermo, Viale delle Scienze, Ed. 17, 90128 Palermo, Italy. E-mail: serena.riela@unipa.it.

[b] Dipartimento di Fisica e Chimica, Università degli Studi di Palermo, Viale delle Scienze, Ed. 17, 90128 Palermo, Italy.

[c] Dipartimento di Scienze Chimiche, Università di Napoli Federico II, Via Cinthia 4, I-80126 Napoli, Italy.

KEYWORDS. Polydopamine, halloysite nanotubes, nanocomposite, environmental remediation.

ABSTRACT. *Hypothesis.* Polydopamine (PDA) is widely used as hydrophilic coating for several applications. However, most of the methods studied to improve or manipulate PDA properties are multistep and time-consuming, and there is a need for versatile strategies aimed at controlling and modifying the properties of PDA. *Experiments.* PDA-halloysite nanocomposites were produced under different oxidation conditions in alkaline and acidic media and were characterized by UV-visible and attenuated total refraction- Fourier Transform Infrared spectroscopies, thermogravimetric analysis, porosimetry, scanning electron microscopy, X-ray diffraction and contact angle measurements against the reference PDA polymer. *Findings.* Inclusion of the inorganic halloysite nanofiller in the PDA component was found to affect the thermal properties of the nanocomposite as well as its structure, depending on the experimental conditions. The ability of the nanocomposites to adsorb organic dyes as possible membrane coatings for environmental remediation was also investigated by different models, suggesting promising applications as adsorbents for the treatment of wastewaters.

INTRODUCTION. Halloysite nanotubes (HNTs) are an aluminosilicate clay, belonging to the kaolin group, which possess predominant hollow tubular morphology and tunable surface chemistry.[1-2] Generally, the inner and outer diameters of the tubes are in the range of 10–30 nm

and 40–70 nm, respectively, while their length is in the range of 0.2–1.5 μm. Halloysite possesses different charged surfaces: positive in the lumen, where aluminum hydroxide is present for the most part and negative on the outer surface, which consists mainly of silicon dioxide (silica). Due to the different chemical composition, HNTs can be selectively functionalized at the inner and/or outer surfaces leading to the synthesis of several nanomaterials of potential practical interest.[3-5] Accordingly, HNTs have found application as nanocontainers for biologically active molecules,[6-10] catalytic supports,[11-13] adsorbent nanomaterials for wastewater decontamination,[14-15] and nanofillers to improve polymer performances, in particular [16-18] cellulose ethers,[19-20] chitosan,[21] alginate[22] and pectin.[23]

Relatively little attention has been directed to investigate the properties of halloysite nanocomposites with polydopamine (PDA), a highly adhesive mussel-inspired eumelanin-type polymer[24] widely used to form hydrophilic coatings for substrate-independent surface functionalization.[25] [25] Like most catecholamine-derived oxidation-products[26] PDA is characterized by catechol-, quinone-, carboxylic and amine-type functionalities within both open chain and cyclized indole units and has found widespread application in the adsorption of metal ions and organic pollutants.[27] However, most of the methods so far investigated to improve or manipulate PDA properties are multistep and time-consuming. For example, the modification of PDA surface is a common method to improve the polymer properties, but commonly it envisages the dopamine polymerization which takes ≈24 h, followed by a secondary modification process that takes another 3–48 h (depending on modification reagents).[28] Therefore, there is a need for versatile strategies aimed at controlling and modifying the properties of PDA for various applications.

So far, few studies have addressed the supramolecular coating of halloysite with PDA[29-34] or the covalent functionalization of the alumina inner lumen with dopamine molecules.[35] A noticeable example of PDA-modified halloysite deals with the preparation of nanocomposites to enhance the properties of polyetherimide (PEI) membranes.[36] Functionalization of the external surface of HNT with PDA led to a nanocomposite that was employed to confer enhanced anti-fouling, bio-fouling and filtration properties to PEI with respect to the pristine membrane. The nanocomposite-modified membrane showed superior capacity to adsorb heavy metal ions, thereby showing rejection towards Pb^{2+} and Cd^{2+}.[36] Other works report the surface modification of HNTs via the self-polymerization of DOPA to obtain materials where the PDA layer acts as

reducing agent and template for the immobilization of metal nanoparticles and enzymes, or to enhance the dispersion ability of HNTs in a polymeric matrix.[37-39]

We report the filler effect of HNTs both on the morphology and on the performances of PDA films. Different PDA materials obtained under both alkaline and acidic conditions were produced and characterized by means of spectroscopic techniques (UV-visible (UV-vis) and attenuated total refraction-Fourier Transform Infrared (ATR-FTIR)), thermogravimetric analysis (TGA), X-ray diffraction (XRD), porosimetry and scanning electron microscopy (SEM) investigations. The performances of the hybrids in the adsorption of organic dyes from an aqueous medium were briefly investigated using Rhodamine B (RB) as a reference dye with a view of probing the PDA-halloysite nanocomposite as membrane coating for environmental remediation.

MATERIALS AND METHODS. Dopamine hydrochloride (≤ 100%), potassium periodate (≥ 99.8%) and halloysite nanotubes were purchased from Sigma-Aldrich and used without further purification. Rhodamine B (RB) (≥ 95%) was purchased from Carlo Erba.

UV-visible measurements were performed using a Beckmann DU 650 spectrometer.

The morphologies of the nanocomposites were studied using an ESEM FEI QUANTA 200F microscope. Before each experiment, the surface of the sample was coated with gold in argon by means of an Edwards Sputter Coater S150A to avoid charging under electron beam treatment. The measurements were carried out in high-vacuum mode ($<6 \times 10^{-4}$ Pa) for the powders and in low-vacuum mode for the film for simultaneous secondary electrons. The energy of the beam was 20 keV, and the working distance was 10 mm. Minimal electron dose conditions were employed to avoid damaging the sample.

ATR-FTIR spectra have been acquired by using an FT-IR Bruker Lumos equipped with Platinum ATR. Spectra result from 60 scans in the wavenumber range 4000-600 cm^{-1}, with resolution of 2 cm^{-1}. The baseline correction has been performed by using the OPUS® software.

X-Ray Diffraction (XRD) patterns of HNTs, PDA-b, PDA/HNT-b, PDA–a and PDA/HNT-a samples were collected, in the theta-theta geometry, using a D8 Eco Bruker diffractometer equipped with a Ni filtered Co Kα radiation source (λ = 1.79 Å) and operating at 40 kV and 30 mA (0.02°/step from 5° to 70° and counting time of 5 s/step).

N_2 adsorption-desorption isotherms were registered at 77 K using a Quantachrome Nova 2200 Multi-Station High Speed Gas Sorption Analyzer. Samples were outgassed for 12 h at room

temperature in the degas station. Adsorbed nitrogen volumes were normalized to the standard temperature and pressure. The specific surface area (S_{BET}) was calculated according to the standard BET method (based on the Brunauer-Emmett-Teller theory) in the relative absorption pressure (P/P^0) range from 0.045 to 0.25034.

Thermogravimetry analyses were carried out by means of a Q5000 IR apparatus (TA Instruments). The measurements were conducted under nitrogen atmosphere (the gas flows were set at 25 and 10 cm^3 min^{-1} for the sample and the balance, respectively) from 25 to 700 °C. The heating rate was set at 20 °C min^{-1}.

The wettability of the glass surfaces coated by dopamine based films was investigated through water contact angle measurements, which were conducted by an optical contact angle apparatus (OCA 20, Data Physics Instruments) equipped with a CCD camera with high-resolution power. Data acquisition was performed by SCA 20 software (Data Physics Instruments). The sessile drop method was used to determine the initial water contact angle (θ_i), which corresponds to the angle just after the deposition of the droplet on the surface. The droplet volume was fixed at 10.0 ± 0.5 μL onto the sample surface, while the temperature was set at 25.0 ± 0.1 °C for both the support and the injecting syringe.

Transparency tests in isothermal conditions (25.0 ± 0.1 °C) were performed through an Analytic Jena Specord S 600 BU. The transmission spectra were registered in the range between 400 and 800 nm.

Synthesis of PDA−a and PDA/HNT−a

Dopamine hydrochloride (10.6 mM) or dopamine hydrochloride (10.6 mM) and HNTs (20 wt%) were dispersed in sodium acetate buffer at 50 mM, pH=5.0. The dispersions were stirred under inert atmosphere overnight. Afterwards, potassium periodate (KP) (10 mM), molar ratio dopamine/KP 1:1, was added to the reaction mixture and it was allowed to stir at room temperature in a becker covered with an aluminum foil for 24 h. To obtain PDA films, a glass slide was dipped in the dispersions for 24 h. The dispersions were then centrifuged for 5 min and the supernatant was removed and replaced with pure water until the supernatant was clear (three centrifugation steps were necessary). The powders were then dried overnight in an oven at 40 °C. Similarly, the glass was collected and washed several times with water and dried at room temperature.

Synthesis of PDA–b and PDA/HNT–b

Dopamine hydrochloride (10.6 mM) or dopamine hydrochloride (10.6 mM) and HNTs (20 wt%) were dispersed in TRIS hydrochloride buffer at 50 mM, pH=8.5 in the presence of different concentrations of HNTs (ranging from 0 to 20 wt%). The dispersions were stirred at room temperature in a becker covered with an aluminum foil for 24 h. To obtain PDA films, a glass slide was dipped in the dispersions for 24 h. The dispersions were then centrifuged for 5 min and the supernatant was removed and replaced with pure water until the supernatant was clear (three centrifugation steps were necessary). The powders were then dried overnight in an oven at 40 °C. Similarly, the glass was collected and washed several times with water and dried at room temperature.

Batch adsorption experiments

All adsorption experiments were conducted on sealed vessels containing 5.0 mg of nanocomposite and 2 mL of RB solution (1×10^{-5} M) in deionized water. The obtained dispersions were vigorously vortexed and shaken in a thermostatic shaker with a shaking of 200 rpm at 25 °C. The supernatant was obtained by centrifugation for detecting RB concentration via UV-vis spectrophotometer at the maximum absorption wavelength of 550 nm. The adsorption capacity (RE (%)) was calculated by:

$$RE(\%) = \frac{(C_0 - C_e)}{C_0} \times 100 \quad \text{(Eq. 1)}$$

where C_0 and C_e are initial and equilibrium concentrations of RB (M), respectively.

Adsorption isotherms

The adsorption isotherms of the nanocomposites were obtained by weighing 5 mg of PDA hybrid in the presence of RB solution in a concentration range of $1 \times 10^{-6} - 5 \times 10^{-5}$ M, in deionized water, and shaken in a thermostated shaker with a shaking of 200 rpm for 12 h to reach equilibrium at 298 K. The equilibrium adsorption capacity Q_e (mol g^{-1}) was calculated by the following equation:

$$Q_e = \frac{(C_0 - C_e) \times V}{M} \quad \text{(Eq. 2)}$$

where C_0 and C_e are initial and equilibrium concentrations of RB (M), respectively, M is the weight of HNTs (g) and V is the volume of RB solution (L).

Adsorption kinetics

The batch experiments were carried out for investigating the adsorption kinetics of RB onto nanocomposites at room temperature in deionized water. For all experiments, the PDA nanocomposites (5 ± 0.1 mg) were added into 2 mL solution of RB (1×10^{-5} M). The amount of RB adsorbed at time *t* (q_t, mol g^{-1}) was calculated by the following equation:

$$q_t = \frac{(C_0 - C_t) \times V}{M} \quad \text{(Eq. 3)}$$

where C_0 and C_t are initial and *t* time concentrations of RB (M), respectively, *M* is the weight of HNTs (g) and *V* is the volume of RB solution (L).

RESULTS AND DISCUSSION. Polydopamine nanocomposites (PDA/HNT) were obtained by dopamine polymerization in the presence of pristine HNTs (20 wt%) in TRIS or acetate buffer at pH 8.5 and 5.0, respectively. Use of different pH and oxidizing systems was dictated by the known effects of the polymerization conditions on PDA final structure and properties.[40-41] Preliminarily, dopamine and HNTs were mixed for 24 h at room temperature under constant stirring and inert atmosphere, to obtain colorless and homogeneous dispersions. Subsequently, oxidation was started either by allowing O_2 into the mixture at pH 8.5, or by adding KIO_4 as the oxidant at pH 5.0 on a 1:1 molar basis. Nanocomposites obtained at pH 8.5, i.e. under basic conditions, were referred to as PDA/HNT–b whereas those obtained by KIO_4 oxidation at acidic pH were referred to as PDA/HNT–a (Scheme 1). The course of dopamine oxidation in the presence of HNTs at pH 8.5 or 5.0 was monitored spectrophotometrically against reference mixtures in the absence of HNTs. In all cases, the progressive darkening of the dispersions resulted eventually in precipitation of a black eumelanin-like PDA polymer (see SI).[40-42]

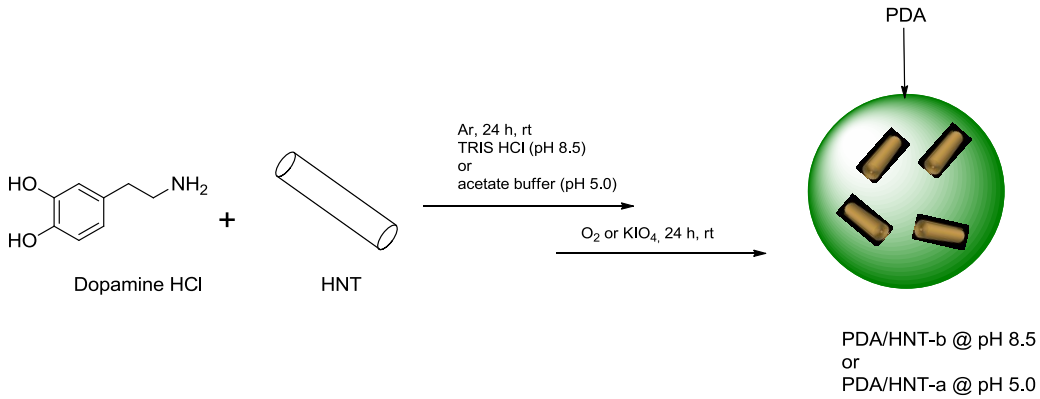

Scheme 1. Schematic representation of the synthesis of PDA nanocomposites.

Figure 1 compares the thermogravimetric (TG) curves of the PDA/HNT hybrids with those of the corresponding PDA samples obtained under the same acidic and basic conditions (PDA-a and PDA-b, respectively).

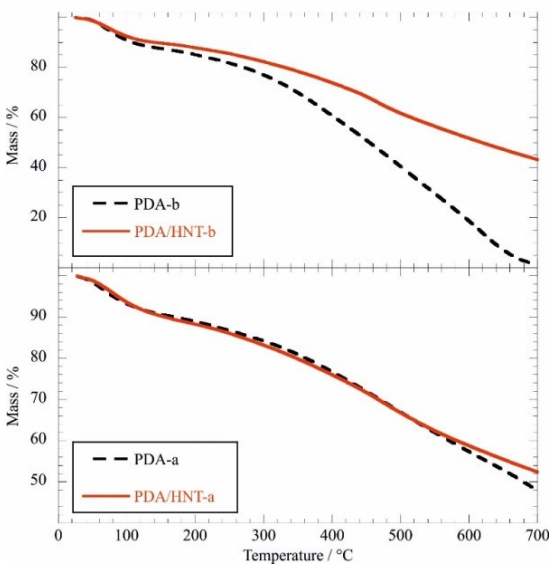

Figure 1. Thermogravimetric curves for PDA/HNT-a and PDA/HNT-b samples against PDA controls under both acidic and alkaline oxidation conditions.

Table 1 indicates a marked loss of water between 25 and 150 °C, which was not affected by HNTs.

Table 1. Thermogravimetric parameters for pure dopamine samples and the dopamine/HNT hybrids.[a]

Sample	$ML_{25\text{-}150}$ / wt%	MR_{700}/ wt%	$ML_{200\text{-}700\ (experimental)}$ / wt%	$ML_{200\text{-}700\ (calculated)}$ / wt%
PDA–b	12.4±0.2	1.56±0.03	83.4±1.7	
PDA–a	9.4±0.2	48.1±0.9	41.2±0.8	
PDA/HNT–b	10.3±0.2	35.9±0.7	51.9±1.0	69.6±1.4
PDA/HNT–a	9.7±0.2	52.4±1	37.8±0.8	35.8±0.7

[a] Results correspond to the mean ± standard error mean of three independent assays.

Gradual degradation was then observed from 200 to 700 °C. Determination of the residual matter at 700 °C (MR_{700}) as well as of the mass loss between 200 and 700 °C ($ML_{200\text{-}700}$) showed that decomposition of samples obtained under basic conditions was almost complete compared to those obtained at pH 5.0 (MR_{700} values of 1.5 vs. 48.1 wt%). The presence of HNTs fillers induced an increase in MR_{700} attributed as expected to the inorganic component. Quantitative analysis of $ML_{200\text{-}700}$ values in Table 1 based on stoichiometric composition (80 and 20 wt% for dopamine and HNTs, respectively) allowed to calculate $ML_{200\text{-}700}$ values of the composites by taking into account the mass loss of pure HNTs (14.5 wt%).[43] Interestingly, whereas the experimental $ML_{200\text{-}700}$ value was close to the calculated one for PDA/HNT-a, ruling out thermal stabilization effects generated by the inorganic filler, the experimental $ML_{200\text{-}700}$ value for PDA/HNT-b was much larger, denoting a thermal stabilization effect caused by HNTs.

Diffraction patterns of the hybrids and the reference polymer samples are reported in Figure 2a (alkaline conditions) and 2b (acidic conditions) compared with HNTs as a reference.

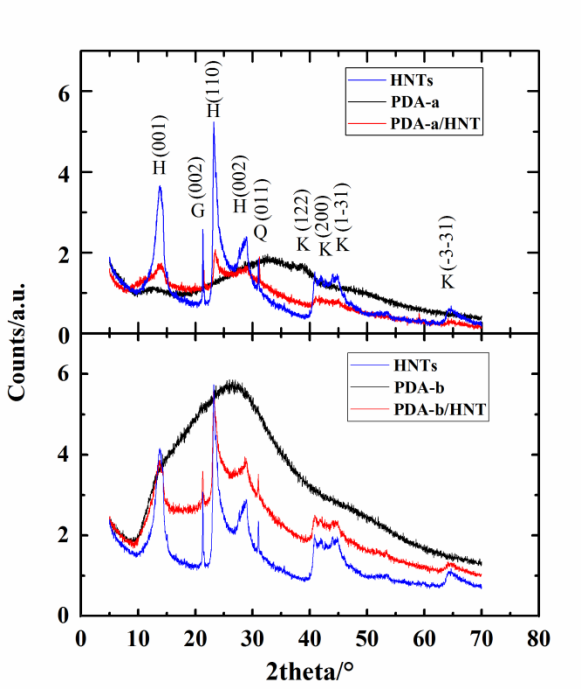

Figure 2. XRD patterns for dopamine samples, their corresponding PDA/HNT samples and HNTs as reference. H, halloysite; Q, quartz; K, kaolinite; G, gibbsite. The diffraction pattern of HNTs shows all the diffraction peaks ascribable to (001), (100), (002) and (110) crystal planes of halloysite, together with peaks of quartz and anatase coherently with the structure of halloysite-(7A).[13, 44]

Data indicated a significant effect of pH on PDA structure.[45-46] In particular, PDA–b displayed the typical pattern of an amorphous polymer whilst PDA–a was apparently organized in crystallites suggesting different local organization of polymer chains. It is possible that this difference reflects the lower degree of intramolecular cyclization that is known to occur under acidic conditions as a consequence of amine chain protonation.[47]

The pattern of PDA/HNT–b was apparently a simple algebraic combination of the patterns of HNTs and PDA–b. Conversely, in the case of PDA/HNT–a, the decrease in the intensity of the (001) peak and the appearance of a shoulder suggested an alteration of the crystal structure of HNTs due to a higher d_{100} spacing among aluminosilicate planes, in agreement with literature.[48] This observation can be rationalized in terms of a swelling process promoted by water and dopamine in the acidic environment following generation of hydrogen bond interactions or coordination between the catechol or $–NH_2$ groups of dopamine and the halloysite surface.

ATR-FTIR analysis (Figure 3) revealed well-documented spectral features for PDA and HNTs (see SI).[41] At first sight, the spectra of the composites showed bands characteristic of both HNTs

and PDA. However, on closer inspection, a shift in the position of the band at ca. 1030 cm^{-1} was observed along with a change in shape. In the case of the PDA/HNT–b composite the band appeared to be the convolution of two contributions ascribed to the asymmetric stretching in-plane Si–O–Si, whereas the contribution at ca. 1010 cm^{-1} was apparently suppressed for the PDA/HNT–a composite. This observation suggested that the main interactions involve the Si–O–Si groups of HNTs.

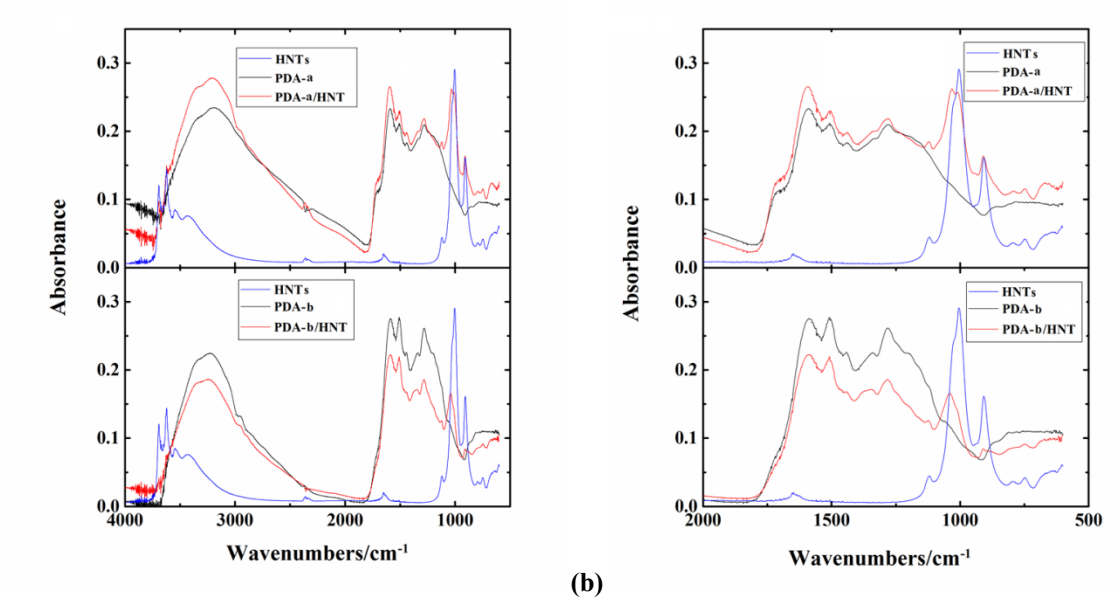

Figure 3. ATR-FTIR spectra of (a) HNTs, PDA–b, PDA/HNT–b, PDA–a and PDA/HNT–a and (b) expanded 2000 – 500 cm^{-1} region.

PDA polymers displayed different morphology depending on the polymerization conditions (Figures 4a and 4c). At pH 5.0 PDA nanospheres proved to be smaller than those obtained at pH 8.5, with a more compact and uniform structure of the polymer.

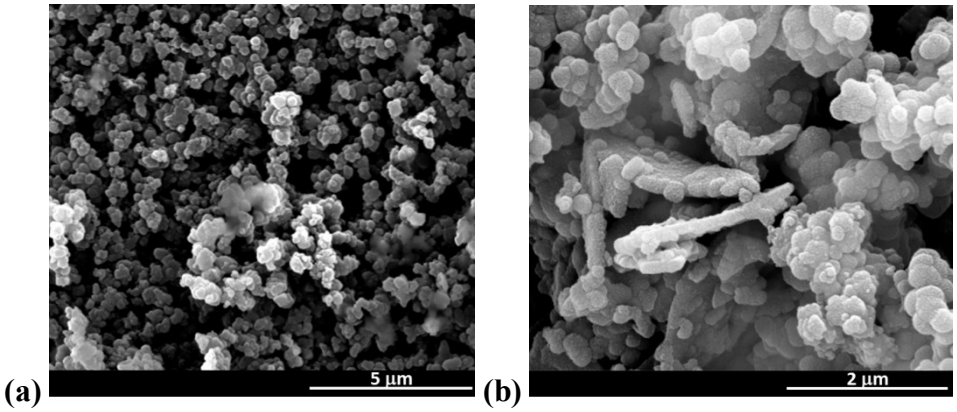

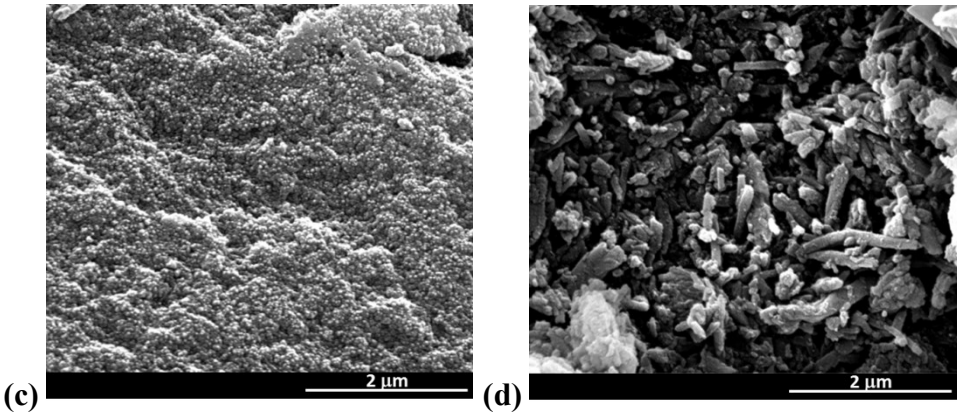

Figure 4. SEM images of (a) PDA–b; (b) PDA/HNT–b, (c) PDA–a and (d) PDA/HNT–a.

Nitrogen adsorption-desorption isotherms were then obtained to gain insights into the specific surface area (S_{BET}). The resulting values obtained for each sample are reported in Table 2.

Table 2. Textural parameters determined by N_2 adsorption/desorption measurements for HNTs, PDA–b, PDA/HNT–b, PDA–a and PDA/HNT–a.[a]

Entry	Sample	BET Surface area (m^2 g^{-1})	Pore volume BJH (cc g^{-1})	Pore Diameter BJH (Å)
1	HNTs	63.8 ± 0.3	0.14 ± 0.02	37.6 ± 0.3
2	PDA–a	0.031 ± 0.001	0.005 ± 0.001	42.5 ± 0.2
3	PDA/HNT–a	2.6 ± 0.2	0.012 ± 0.003	39.7 ± 0.3
4	PDA–b	9.6 ± 0.3	0.028 ± 0.005	42. 9 ± 0.3
5	PDA/HNT–b	4.7 ± 0.2	0.021 ± 0.002	39.8 ± 0.3

[a] Results correspond to the mean ± standard error mean of three independent assays.

The halloysite surface area is comparable with values reported in literature.[49] The surface area values for the PDA samples proved to be in fairly good agreement with the morphology data. Higher values were consistently determined for PDA–b which was made up of tightly aggregated nanospheres (Figure 4a) than for PDA–a, which was significantly more compact (Figure 4c).

Interestingly, whereas the surface area increased in the nanocomposite PDA–a, it markedly decreased (more than halved) in the case of PDA–b. Coherently with the XRD and ATR-FTIR this could be ascribed to different interactions among the components: whereas in the case of PDA/HNT–a the presence of the nanofiller, respect to PDA-a, caused a more or less extensive local disruption of the compact organic aggregate (entries 2 and 3), in the case of PDA/HNT–b the presence of the inorganic component, respect to PDA-b, induced a more regular and compact aggregation over the halloysite surface (entries 4 and 5).

The surface area values proved to be coherent with morphology data inferred from SEM images (Figures 4b and 4d). Images showed that the characteristic length and tubular shape of HNTs are preserved in both nanocomposites. However, at pH 8.5 the HNTs appear to be uniformly dispersed in the PDA matrix, looking as tubes covered by PDA (Figure 4b), whereas in acidic medium they seem to be more aggregated and wrapped by the polymer (Figure 4d).

Such different morphologies could be explained on the basis of the different interactions that may be operative among the HNTs at different pH. At alkaline pH, e.g. 8.5, the Si–OH groups on the outer surface of the tubes are expectedly deprotonated to cause the maximum negative charge.[50] As a consequence, electrostatic interactions among the tubes are minimized with increased dispersion. In consequence, dopamine polymerization may occur in part on the nanotube surface causing them to be covered by PDA.

Conversely, at pH 5.0, i.e. below the isoelectric point of HNTs (pH ca. 6.5),[50] the tubes exist in their zwitteronic form, whereby electrostatic interactions with the growing PDA polymer may be less significant on account of a different tendency of the tubes to aggregate and of PDA formation processes that are less affected by HNTs surface.

Adsorption measurements

The adsorption capacity of the PDA nanocomposites for rhodamine B (RB), chosen as a fluorescent probe at pH 7.4, was investigated next. Both PDA/HNT–b and PDA/HNT–a nanocomposites showed similar or greater adsorption capacity than reference PDA samples (see SI).

On this basis, the adsorption capacity of the nanocomposites was determined by adsorption isotherm experiments. Figure 5 reports the equilibrium amount of dye adsorbed onto the

nanocomposite (Q_e, mol g^{-1}) as a function of the equilibrium dye concentration in solution (C_e, mol L^{-1}).

Data indicated a lower amount of dye adsorbed on PDA/HNT–a. This could be due to the effect of the pH of the medium on PDA buildup and mode of polymerization.[40]

Both the Langmuir and the Freundlich models were used to analyze the experimental data.[51] Table 3 showed that adsorption data related to PDA/HNT–b are better fitted by the Freundlich model, suggesting heterogeneous nanocomposite and multi-molecular layer adsorption according to SEM data. The value of *n* is larger than 1, which indicates the favorable nature of adsorption and a physical process.[52] Conversely, for PDA/HNT–a a monolayer adsorption was determined, the adsorption data being better fitted by the Langmuir model. These results support the view that at pH 5.0 aggregates of HNTs are embedded into a PDA matrix.[53]

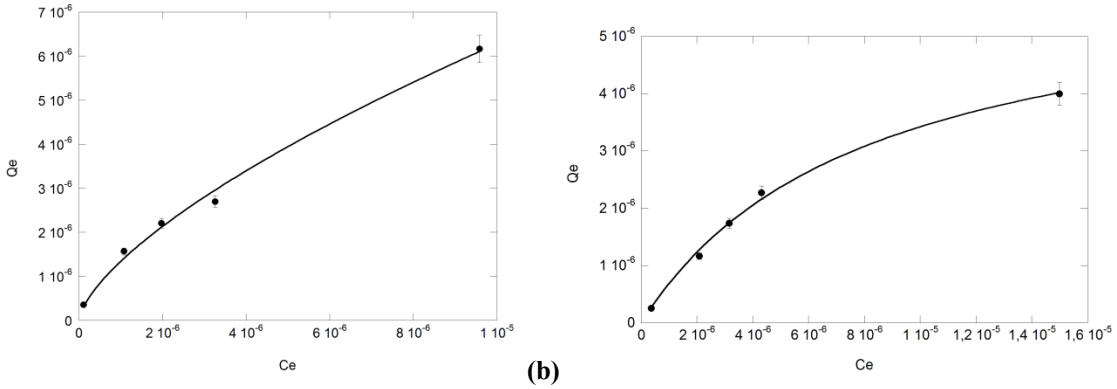

Figure 5. Adsorption isotherms of RB on (a) PDA/HNT–b and (b) PDA/HNT–a in deionized water (results correspond to the mean ± standard error mean of three independent assays).

Table 3. Parameters of Langmuir and Freundlich isotherm models for RB adsorption on the hybrid nanocomposites.[a]

	Langmuir $Q_e = \frac{K_L Q_m C_e}{1 + K_L C_e}$			**Freundlich** $Q_e = K_F C_e^{1/2}$		
	Q_m (mol g^{-1})	K_L (L mol^{-1})	R^2	K_F (mol g^{-1} (mol L^{-1})$^{1/n}$)	*n*	R^2
PDA/HNT–b	$(1.8\pm0.7)\times10^{-5}$	$(6\pm3)\times10^{4}$	0.973	0.014±0.006	1.50±0.08	0.994
PDA/HNT–a	$(2.48\pm0.07)\times10^{-3}$	$(1.3\pm0.1)\times10^{5}$	0.997	0.002±0.001	1.7±0.2	0.979

[a] Results correspond to the mean ± standard error mean of three independent assays.

To gain further insight into the adsorption mechanisms, the kinetics of rhodamine B adsorption onto PDA/HNT−b and PDA/HNT−a were investigated (see SI). It was found that dye adsorption on PDA/HNT−a increases rapidly in the first 200 min and then slows down to reach equilibrium. The rapid initial adsorption is due to the presence of a compact PDA surface with a large number of adsorption sites on the surface of the nanocomposite. As the surface active sites are gradually occupied, the adsorption rates slow down and finally reach equilibrium. At pH 8.5 the kinetics of RB adsorption are apparently slower and the equilibrium is not reached over as long as 1000 minutes.

The kinetic data were fitted by the intraparticle diffusion model (Weber-Morris model) and by a pseudo-second-order kinetic model given by Langergren and Svenska to analyze rate controlling steps which affect the adsorption process.

The experimental data were found to be better fitted by the pseudo-second order model as far as PDA/HNT−b is concerned, whereas the kinetic adsorption of PDA/HNT−a better fitted the Weber Morris model. On the contrary, the kinetic adsorption of RB onto pristine HNTs follows the pseudo-second order model, according to the presence of two different surfaces interacting with the dye, whereas the experimental data of PDA/HNT-a and PDA/HNT-b are better fitted by the intraparticle diffusion model (Table S.1).

These results are consistent with the different morphologies reported below (Table 4).

Table 4. Adsorption Kinetic Parameters of RB onto PDA nanocomposites.[a]

	Pseudo second order $\frac{t}{Q_t} = \frac{t}{Q_e} + \frac{1}{k_2 Q_e^2}$			**Weber Morris** $Q_t = k_d t^{0.5} + L$	
	q_e (mol g^{-1})	k_2 (g mol^{-1} min^{-1})	R^2	k_d (g mol^{-1} $min^{-0.5}$)	R^2
PDA/HNT−b	$(1.37\pm0.01)\times10^{-6}$	$(4.2\pm0.6)\times10^{5}$	0.998	n.a.[b]	n.a.[b]
PDA/HNT−a	$(1.45\pm0.02)\times10^{-6}$	$(6.8\pm0.6)\times10^{3}$	0.985	$(2.63\pm0.03)\times10^{-6}$	0.992

[a] Results correspond to the mean ± standard error mean of three independent assays.
[b] Weber Morris model is not successful.

Coating of glass surfaces with PDA/HNT nanocomposites.

SEM images of PDA films produced at pH 5.0 or 8.5 with or without HNTs showed morphologies reflecting those of the powders (Figure 6). Figures 6b and 6d indicate both dispersed (red arrows in the Figure 6b) or aggregated HNTs, respectively, in line with the preceding findings.

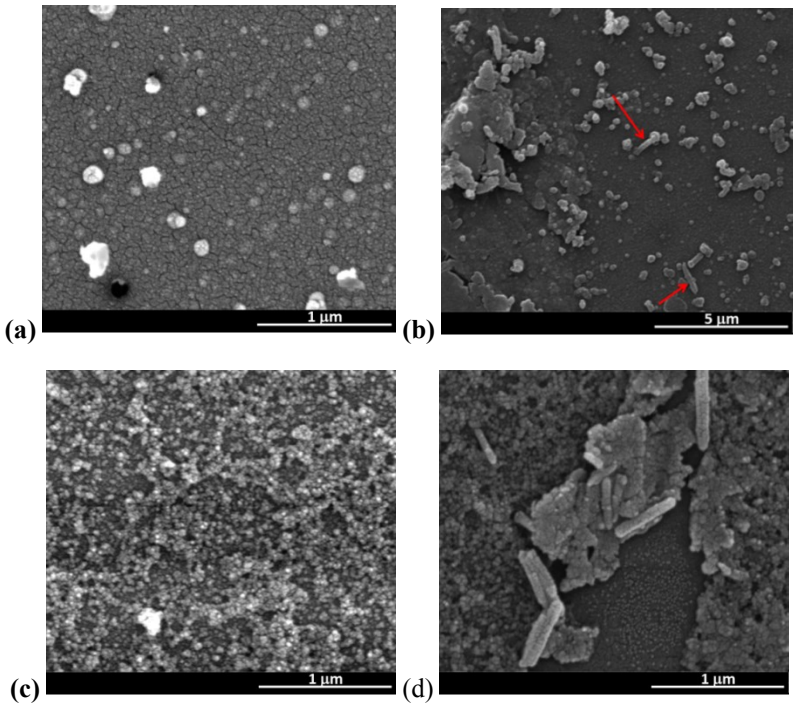

Figure 6. SEM images of (a) PDA-b; (b) PDA/HNT–b, (c) PDA-a and (d) PDA/HNT–a films.

The morphological features of the PDA/HNT nanocomposites affected their macroscopic characteristics in terms of transparency and wettability. As evidenced by the transmission spectra (Figure 7), the coating of the glass substrate with PDA based films produces a reduction of its transparency.

As a general result, transmittance increased with the wavelength, in agreement with the light scattering determined by the nanoparticles. The decrease in glass transparency proved to be lower for PDA-b compared to PDA–a. As expected, addition of HNTs produced a further transparency decrease of the coated glass samples. This effect was observed in nanocomposite materials containing HNTs within the polymeric matrix.[54]

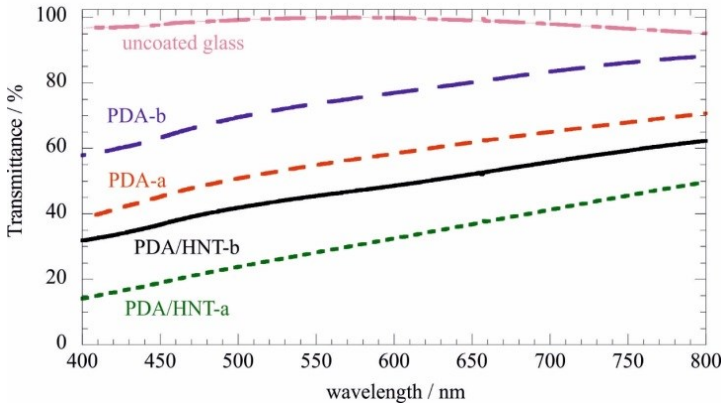

Figure 7. Transmittance as function of the wavelength for uncoated and coated glass.

Table 5 collects the transmittance data at 600 nm (T_{600}) as well as the ratio between the transmittance percentages at 800 and 400 nm (T_{800}/T_{400}) for the coated glass samples.

The T_{600} values revealed that the addition of HNTs produces similar reduction effects on the polydopamines transparency at 600 nm. Compared to the corresponding pure polydopamine, we observed that PDA/HNT–b and PDA/HNT–a exhibit T_{600} decreases of 28 and 26 %, respectively. Additionally, we detected that the presence of HNTs induces an enhancement of the T_{800}/T_{400} ratio for both polydopamines. These results highlight that the transparency of the composite materials is more sensitive to wavelength variations. It should be noted that this effect is more relevant for PDA/HNT–a material.

The surface properties of the films were investigated by determining the water contact angles of the coated glass specimens.

A slight increase in the water contact angle was determined in the presence of the HNTs filler in both cases. This effect cannot be attributed to variations of the chemical composition of the surfaces, due to the hydrophilic character of halloysite. Rather, it is possible that it follows from the enhancement of the surface roughness caused by HNTs. Similar results were observed for polymer/HNT nanocomposites with the nanotubes dispersed at the interface.[19]

Table 5. Transmittance data for coated glass samples.[a]

	$T_{600\ nm}$ (%)	T_{800}/T_{400}
PDA–b	77.0 ± 1.5	1.52 ± 0.04

PDA–a	58 ± 1	1.84 ± 0.07
PDA/HNT–b	49 ± 1	1.96 ± 0.09
PDA/HNT–a	32.0 ± 0.6	3.5 ± 0.3

[a] Results correspond to the mean ± standard error mean of three independent assays.

CONCLUSIONS

To date most of the methods commonly adopted to improve polydopamine (PDA) properties are multi-step and time consuming. Therefore, there is a need for versatile strategies aimed at controlling and modifying the properties of PDA for various applications.

Halloysite nanotubes (HNTs) are usefully used to improve the physico-chemical properties of polymers. Previous studies dealt with the use of PDA as coating for HNTs surface.[36-37] So far, no studies were focused on the use of HNTs as filler for PDA matrix.

Herein, PDA/HNT nanocomposites were obtained under both acidic and alkaline oxidation conditions and were characterized for the physicochemical properties.

The most significant findings are as follows.

a) HNT fillers can interact in different ways with PDA structure depending on the pH of the medium and can produce complex effects on nanocomposite morphology.

b) HNTs markedly increased the thermal stability of PDA samples on thermogravimetric analysis.

c) PDA/HNT nanocomposites displayed similar or slightly enhanced adsorption capacity for the organic dye Rhodamine B relative to PDA, depending on the nature of the nanocomposite.

d) PDA/HNT nanocomposites coated on a glass surface impart morphologies to the substrate similar to those of the bulk polymers and affect transparency and wettability of the nanocomposite by enhancing surface roughness. In all cases the effects are more relevant for PDA/HNT–a material respect to PDA/HNT–b.

These results point to HNTs incorporation as a promising strategy to modify and tailor PDA film properties for diverse applications, ranging from enhancement of adsorption to surface modification.

Supporting Information. Kinetic of polydopamine polymerization, ATR-FTIR investigations of pristine PDA and HNTs, adsorption capacities of the different nanocomposites for RB, kinetic adsorption of RB on PDA/HNT nanocomposites, kinetic parameters of RB adsorption on HNT, PDA–a and PDA–b, contact angle measurements of PDA nanocomposite films.

ACKNOWLEDGMENT

The work was financially supported by the University of Palermo and was carried out in the frame of the PRIN2017-2017YJMPZN project.

REFERENCES

1. Ma, W.; Wu, H.; Higaki, Y.; Takahara, A., Halloysite Nanotubes: Green Nanomaterial for Functional Organic-Inorganic Nanohybrids. *Chem. Rec.* **2018,** *18* (7), 986-999.
2. Zhao, X.; Zhou, C.; Lvov, Y.; Liu, M., Clay Nanotubes Aligned with Shear Forces for Mesenchymal Stem Cell Patterning. *Small* **2019**.
3. Tharmavaram, M.; Pandey, G.; Rawtani, D., Surface modified halloysite nanotubes: A flexible interface for biological, environmental and catalytic applications. *Adv. Colloid Interface Sci.* **2018,** *261*, 82-101.
4. Massaro, M.; Cavallaro, G.; Colletti, C. G.; Lazzara, G.; Milioto, S.; Noto, R.; Riela, S., Chemical modification of halloysite nanotubes for controlled loading and release. *J. Mater. Chem. B* **2018,** *6* (21), 3415-3433.
5. Massaro, M.; Colletti, C. G.; Guernelli, S.; Lazzara, G.; Liu, M.; Nicotra, G.; Noto, R.; Parisi, F.; Pibiri, I.; Spinella, C.; Riela, S., Photoluminescent hybrid nanomaterials from modified halloysite nanotubes. *J. Mater. Chem. C* **2018,** *6* (27), 7377-7384.
6. Massaro, M.; Barone, G.; Biddeci, G.; Cavallaro, G.; Di Blasi, F.; Lazzara, G.; Nicotra, G.; Spinella, C.; Spinelli, G.; Riela, S., Halloysite nanotubes-carbon dots hybrids multifunctional nanocarrier with positive cell target ability as a potential non-viral vector for oral gene therapy. *J. Colloid Interface Sci.* **2019**.
7. Tarasova, E.; Naumenko, E.; Rozhina, E.; Akhatova, F.; Fakhrullin, R., Cytocompatibility and uptake of polycations-modified halloysite clay nanotubes. *Appl. Clay Sci.* **2019,** *169*, 21-30.
8. Massaro, M.; Riela, S., Organo-clay nanomaterials based on halloysite and cyclodextrin as carriers for polyphenolic compounds. *J. Funct. Biomater.* **2018,** *9* (4).
9. Massaro, M.; Campofelice, A.; Colletti, C. G.; Lazzara, G.; Noto, R.; Riela, S., Functionalized halloysite nanotubes: Efficient carrier systems for antifungine drugs. *Appl. Clay Sci.* **2018,** *160*, 186-192.

10. Massaro, M.; Cavallaro, G.; Colletti, C. G.; D'Azzo, G.; Guernelli, S.; Lazzara, G.; Pieraccini, S.; Riela, S., Halloysite nanotubes for efficient loading, stabilization and controlled release of insulin. *J. Colloid Interface Sci.* **2018,** *524*, 156-164.
11. Sidorenko, A. Y.; Kravtsova, A. V.; Aho, A.; Heinmaa, I.; Volcho, K. P.; Salakhutdinov, N. F.; Agabekov, V. E.; Yu. Murzin, D., Acid-modified Halloysite Nanotubes as a Stereoselective Catalyst for Synthesis of 2H-Chromene Derivatives by the Reaction of Isopulegol with Aldehydes. *ChemCatChem* **2018,** *10* (18), 3950-3954.
12. Mishra, G.; Mukhopadhyay, M., TiO_2 decorated functionalized halloysite nanotubes (TiO_2@HNTs) and photocatalytic PVC membranes synthesis, characterization and its application in water treatment. *Sci. Rep.* **2019,** *9* (1).
13. Massaro, M.; Colletti, C. G.; Fiore, B.; La Parola, V.; Lazzara, G.; Guernelli, S.; Zaccheroni, N.; Riela, S., Gold nanoparticles stabilized by modified halloysite nanotubes for catalytic applications. *Appl. Organomet. Chem.* **2019,** *33* (3).
14. Massaro, M.; Colletti, C. G.; Buscemi, G.; Cataldo, S.; Guernelli, S.; Lazzara, G.; Liotta, L. F.; Parisi, F.; Pettignano, A.; Riela, S., Palladium nanoparticles immobilized on halloysite nanotubes covered by a multilayer network for catalytic applications. *New J. Chem.* **2018,** *42* (16), 13938-13947.
15. Gładysz-Płaska, A.; Majdan, M.; Tarasiuk, B.; Sternik, D.; Grabias, E., The use of halloysite functionalized with isothiouronium salts as an organic/inorganic hybrid adsorbent for uranium(VI) ions removal. *J. Hazard. Mater.* **2018,** *354*, 133-144.
16. Sharma, S.; Singh, A. A.; Majumdar, A.; Butola, B. S., Tailoring the mechanical and thermal properties of polylactic acid-based bionanocomposite films using halloysite nanotubes and polyethylene glycol by solvent casting process. *J. Mater. Sci.* **2019,** *54* (12), 8971-8983.
17. Kumar, A.; Zo, S. M.; Kim, J. H.; Kim, S. C.; Han, S. S., Enhanced physical, mechanical, and cytocompatibility behavior of polyelectrolyte complex hydrogels by reinforcing halloysite nanotubes and graphene oxide. *Compos. Sci. Technol.* **2019,** *175*, 35-45.
18. De Silva, R. T.; Dissanayake, R. K.; Mantilaka, M. M. M. G. P. G.; Wijesinghe, W. P. S. L.; Kaleel, S. S.; Premachandra, T. N.; Weerasinghe, L.; Amaratunga, G. A. J.; De Silva, K. M. N., Drug-Loaded Halloysite Nanotube-Reinforced Electrospun Alginate-Based Nanofibrous Scaffolds with Sustained Antimicrobial Protection. *ACS Appl. Mater. Interf.* **2018,** *10* (40), 33913-33922.
19. Bertolino, V.; Cavallaro, G.; Lazzara, G.; Merli, M.; Milioto, S.; Parisi, F.; Sciascia, L., Effect of the Biopolymer Charge and the Nanoclay Morphology on Nanocomposite Materials. *Ind. Eng. Chem. Res.* **2016,** *55* (27), 7373-7380.
20. Guo, S.; Zhao, K.; Feng, Z.; Hou, Y.; Li, H.; Zhao, J.; Tian, Y.; Song, H., High performance liquid crystalline bionanocomposite ionogels prepared by in situ crosslinking of cellulose/halloysite nanotubes/ionic liquid dispersions and its application in supercapacitors. *Appl. Surf. Sci.* **2018,** *455*, 599-607.
21. Liu, M.; Wu, C.; Jiao, Y.; Xiong, S.; Zhou, C., Chitosan–halloysite nanotubes nanocomposite scaffolds for tissue engineering. *J. Mater. Chem. B* **2013,** *1* (15), 2078-2089.
22. Shankar, S.; Kasapis, S.; Rhim, J. W., Alginate-based nanocomposite films reinforced with halloysite nanotubes functionalized by alkali treatment and zinc oxide nanoparticles. *Int. J. Biol. Macromol.* **2018,** *118*, 1824-1832.
23. Makaremi, M.; Pasbakhsh, P.; Cavallaro, G.; Lazzara, G.; Aw, Y. K.; Lee, S. M.; Milioto, S., Effect of Morphology and Size of Halloysite Nanotubes on Functional Pectin

Bionanocomposites for Food Packaging Applications. *ACS Appl. Mater. Interf.* **2017,** *9* (20), 17476-17488.
24. Ryu, J. H.; Messersmith, P. B.; Lee, H., Polydopamine Surface Chemistry: A Decade of Discovery. *ACS Appl. Mater. Interf.* **2018,** *10* (9), 7523-7540.
25. Liu, Y.; Ai, K.; Lu, L., Polydopamine and Its Derivative Materials: Synthesis and Promising Applications in Energy, Environmental, and Biomedical Fields. *Chem. Rev.* **2014,** *114* (9), 5057-5115.
26. d'Ischia, M.; Palumbo, A.; Prota, G., Adrenalin oxidation revisited. New products beyond the adrenochrome stage. *Tetrahedron* **1988,** *44* (20), 6441-6446.
27. Liu, R.; Dai, L.; Si, C.-L., Mussel-Inspired Cellulose-Based Nanocomposite Fibers for Adsorption and Photocatalytic Degradation. *ACS Sustain. Chem. Eng.* **2018,** *6* (11), 15756-15763.
28. Zeng, Y.; Du, X.; Hou, W.; Liu, X.; Zhu, C.; Gao, B.; Sun, L.; Li, Q.; Liao, J.; Levkin, P. A.; Gu, Z., UV-Triggered Polydopamine Secondary Modification: Fast Deposition and Removal of Metal Nanoparticles. *Adv. Funct. Mater.* **2019,** *0* (0), 1901875.
29. Zeng, G.; Ye, Z.; He, Y.; Yang, X.; Ma, J.; Shi, H.; Feng, Z., Application of dopamine-modified halloysite nanotubes/PVDF blend membranes for direct dyes removal from wastewater. *Chem. Eng. J.* **2017,** *323*, 572-583.
30. Sadjadi, S.; Lazzara, G.; Malmir, M.; Heravi, M. M., Pd nanoparticles immobilized on the poly-dopamine decorated halloysite nanotubes hybridized with N-doped porous carbon monolayer: A versatile catalyst for promoting Pd catalyzed reactions. *J. Catal.* **2018,** *366*, 245-257.
31. Liu, Y.; Tu, W.; Chen, M.; Ma, L.; Yang, B.; Liang, Q.; Chen, Y., A mussel-induced method to fabricate reduced graphene oxide/halloysite nanotubes membranes for multifunctional applications in water purification and oil/water separation. *Chem. Eng. J.* **2018,** *336*, 263-277.
32. Kang, H.; Liu, X.; Zhang, S.; Li, J., Functionalization of halloysite nanotubes (HNTs) via mussel-inspired surface modification and silane grafting for HNTs/soy protein isolate nanocomposite film preparation. *RSC Adv.* **2017,** *7* (39), 24140-24148.
33. Feng, J.; Fan, H.; Zha, D. A.; Wang, L.; Jin, Z., Characterizations of the formation of polydopamine-coated halloysite nanotubes in various pH environments. *Langmuir* **2016,** *32* (40), 10377-10386.
34. Ganguly, S.; Das, N. C., Synthesis of Mussel Inspired Polydopamine Coated Halloysite Nanotubes Based Semi-IPN: An Approach to Fine Tuning in Drug Release and Mechanical Toughening. *Macromol. Symp.* **2018,** *382* (1), 1800076.
35. Yah, W. O.; Xu, H.; Soejima, H.; Ma, W.; Lvov, Y.; Takahara, A., Biomimetic dopamine derivative for selective polymer modification of halloysite nanotube lumen. *J. Am. Chem. Soc.* **2012,** *134* (29), 12134-12137.
36. Hebbar, R. S.; Isloor, A. M.; Ananda, K.; Ismail, A. F., Fabrication of polydopamine functionalized halloysite nanotube/polyetherimide membranes for heavy metal removal. *J. Mater. Chem. A* **2016,** *4* (3), 764-774.
37. Chao, C.; Liu, J.; Wang, J.; Zhang, Y.; Zhang, B.; Zhang, Y.; Xiang, X.; Chen, R., Surface Modification of Halloysite Nanotubes with Dopamine for Enzyme Immobilization. *ACS Appl. Mater. Interf.* **2013,** *5* (21), 10559-10564.
38. Luo, C.; Zou, Z.; Luo, B.; Wen, W.; Li, H.; Liu, M.; Zhou, C., Enhanced mechanical properties and cytocompatibility of electrospun poly(l-lactide) composite fiber membranes assisted by polydopamine-coated halloysite nanotubes. *Appl. Surf. Sci.* **2016,** *369*, 82-91.

39. Ren, Y.; Zhang, S.; Wan, X.; Zhan, Y.; Zhang, J.; He, Y., High-performance dielectric poly(arylene ether nitrile)/Ag nanoparticles decorated halloysites nanotube composites through modified bio-inspired method and synergistic effect. *Polymer Engineering & Science* **2018,** *58* (12), 2227-2236.
40. Ponzio, F.; Barthès, J.; Bour, J.; Michel, M.; Bertani, P.; Hemmerlé, J.; d'Ischia, M.; Ball, V., Oxidant Control of Polydopamine Surface Chemistry in Acids: A Mechanism-Based Entry to Superhydrophilic-Superoleophobic Coatings. *Chem. Mater.* **2016,** *28* (13), 4697-4705.
41. Schneider, A.; Hemmerlé, J.; Allais, M.; Didierjean, J.; Michel, M.; d'Ischia, M.; Ball, V., Boric Acid as an Efficient Agent for the Control of Polydopamine Self-Assembly and Surface Properties. *ACS Appl. Mater. Interf.* **2018,** *10* (9), 7574-7580.
42. Alfieri, M.; Panzella, L.; Oscurato, S.; Salvatore, M.; Avolio, R.; Errico, M.; Maddalena, P.; Napolitano, A.; d'Ischia, M., The Chemistry of Polydopamine Film Formation: The Amine-Quinone Interplay. *Biomimetics* **2018,** *3* (3), 26.
43. Cavallaro, G.; Milioto, S.; Parisi, F.; Lazzara, G., Halloysite Nanotubes Loaded with Calcium Hydroxide: Alkaline Fillers for the Deacidification of Waterlogged Archeological Woods. *ACS Appl. Mater. Interf.* **2018,** *10* (32), 27355-27364.
44. Delvaux, B.; Theng, B.; Righi, D.; Joussein, E.; Churchman, J.; Petit, S., Halloysite clay minerals — a review. *Clay Miner.* **2005,** *40* (4), 383-426.
45. Ho, C.-C.; Ding, S.-J., The pH-controlled nanoparticles size of polydopamine for anti-cancer drug delivery. *Journal of Materials Science: Materials in Medicine* **2013,** *24* (10), 2381-2390.
46. Bisaglia, M.; Mammi, S.; Bubacco, L., Kinetic and Structural Analysis of the Early Oxidation Products of Dopamine: ANALYSIS OF THE INTERACTIONS WITH α-SYNUCLEIN. *J. Biol. Chem.* **2007,** *282* (21), 15597-15605.
47. Della Vecchia, N. F.; Avolio, R.; Alfè, M.; Errico, M. E.; Napolitano, A.; d'Ischia, M., Building-Block Diversity in Polydopamine Underpins a Multifunctional Eumelanin-Type Platform Tunable Through a Quinone Control Point. *Adv. Funct. Mater.* **2013,** *23* (10), 1331-1340.
48. Feng, J.; Fan, H.; Zha, D.-a.; Wang, L.; Jin, Z., Characterizations of the Formation of Polydopamine-Coated Halloysite Nanotubes in Various pH Environments. *Langmuir* **2016,** *32* (40), 10377-10386.
49. Gaaz, T. S.; Sulong, A. B.; Kadhum, A. A. H.; Nassir, M. H.; Al-Amiery, A. A., Surface improvement of halloysite nanotubes. *Applied Sciences (Switzerland)* **2017,** *7* (3).
50. Bretti, C.; Cataldo, S.; Gianguzza, A.; Lando, G.; Lazzara, G.; Pettignano, A.; Sammartano, S., Thermodynamics of Proton Binding of Halloysite Nanotubes. *J. Phys. Chem. C* **2016,** *120* (14), 7849-7859.
51. Massaro, M.; Colletti, C. G.; Lazzara, G.; Guernelli, S.; Noto, R.; Riela, S., Synthesis and Characterization of Halloysite–Cyclodextrin Nanosponges for Enhanced Dyes Adsorption. *ACS Sustain. Chem. Eng.* **2017,** *5* (4), 3346-3352.
52. Gereli, G.; Seki, Y.; Murat Kuşoğlu, İ.; Yurdakoç, K., Equilibrium and kinetics for the sorption of promethazine hydrochloride onto K10 montmorillonite. *J. Colloid Interface Sci.* **2006,** *299* (1), 155-162.
53. Fu, J.; Xin, Q.; Wu, X.; Chen, Z.; Yan, Y.; Liu, S.; Wang, M.; Xu, Q., Selective adsorption and separation of organic dyes from aqueous solution on polydopamine microspheres. *J. Colloid Interface Sci.* **2016,** *461*, 292-304.

54. Cavallaro, G.; Lazzara, G.; Milioto, S., Dispersions of Nanoclays of Different Shapes into Aqueous and Solid Biopolymeric Matrices. Extended Physicochemical Study. *Langmuir* **2011,** *27* (3), 1158-1167.